ACS APPLIED MATERIALS & INTERFACES

Research Article

Cite This: ACS Appl. Mater. Interfaces 2018, 10, 15820−15828

www.acsami.org

Ultrasonic Preparation of Porous Silica-Dye Microspheres: Sensors for Quantification of Urinary Trimethylamine *N*-Oxide

Zheng Li and Kenneth S. Suslick*

Department of Chemistry, University of Illinois at Urbana−Champaign, 600 S. Mathews Avenue, Urbana, Illinois 61801, United States

Supporting Information

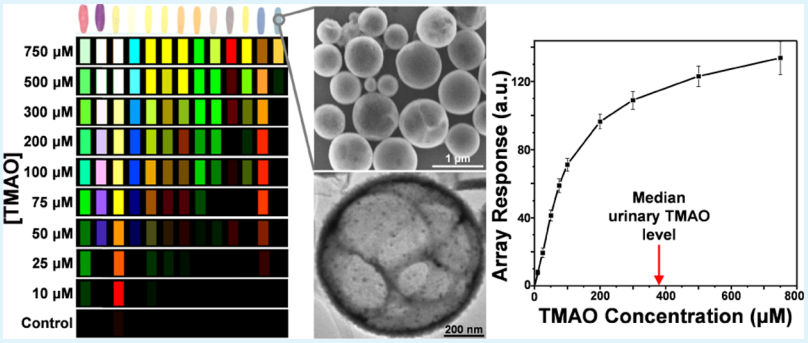

ABSTRACT: Trimethylamine *N*-oxide (TMAO), the *N*-oxide metabolite of trimethylamine (TMA), is a key index in the determination of a wide variety of human cardiac or kidney diseases. A colorimetric sensor array comprising ultrasonically prepared silica-dye microspheres was developed for rapid, portable, and sensitive detection of urinary TMAO. To prepare the sensor array, 13 different organically modified silica (ormosil)-dye composites were synthesized from the hydrolysis/pyrolysis of ultrasonically sprayed organosiloxane precursors under optimized reaction conditions; the resulting products are uniformly sized nanoporous microspheres that are effective colorimetric sensors for various volatile analytes. The effective quantification of aqueous TMAO (which is not volatile) was based on sensing the volatile TMA produced from a simple catalytic reduction of TMAO in situ. RGB color-change patterns from digital images of the sensor array permit precise discrimination among a wide range of TMAO concentrations (10−750 μM) in simulated urine samples; both hierarchical cluster analysis and principal component analysis achieve >99% accuracy in data classification. The calculated limit of detection of urinary TMAO is ∼4 μM, which is substantially below the median level of healthy subjects (∼380 μM). The array of sensors could be simplified to only a couple of strongly responsive elements for the ease of field use, and the process could be developed as a point-of-care tool in combination with digital imaging for the early diagnosis of cardiovascular or kidney diseases from the measurement of fasting urinary level of TMAO.

KEYWORDS: *silica-dye microspheres, ultrasonic spray pyrolysis, colorimetric sensing, sensor array, urinary TMAO, point-of-care device*

1. INTRODUCTION

Trimethylamine *N*-oxide (TMAO), a metabolite produced from choline, betaine, and carnitine by the intestinal microbiota,[1,2] is a key biomarker for a wide variety of human cardiac or kidney diseases[3,4] and recently for colorectal cancer.[5,6] TMAO is a major atherogenic factor that affects cholesterol metabolism in human organs and is indicative of potential risk for stroke, atherosclerosis, coronary artery disease, and heart failure.[7−9] It has recently been reported that direct correlations have been substantially established between fasting blood levels of TMAO and the long-term risk of multiple cardiovascular diseases.[10,11] Given the significant biomedical functions of TMAO, there remains a real clinical demand for new methods for the rapid quantification of TMAO in human serum or urine.

Currently, the commonly used methods for TMAO quantification are GC- or LC-MS[12−16] or NMR[17,18] techniques that generally require long analysis time, high cost, and complicated instrumentation. Given the relative inertness of TMAO in terms of physical or chemical properties (e.g., lack of reactive functionality or redox, low volatility, and low basicity), electrochemical or optical detection of TMAO has not proved viable. Hatton and Gibb[19] reported an enzymatic method for the reduction of TMAO to trimethylamine (TMA) using TMAO reductase, followed by the quantification of resulting TMA vapors using ion chromatography. Haswell and co-workers used the air-sensitive $TiCl_3$ as a reductant coupled to GC analysis of the resultant TMA.[20] This reduction approach to TMAO analysis opens an interesting path, yet its practical application has been limited because of the need to separate

Received: January 18, 2018
Accepted: April 11, 2018
Published: April 25, 2018

DOI: 10.1021/acsami.8b00995
ACS Appl. Mater. Interfaces 2018, 10, 15820−15828

amine analytes, the lack of simplicity, efficiency, and portability of either of these reductions.

Colorimetric array-based sensors, also known as an "optoelectronic nose", as developed by the Suslick group over the past two decades,[21−23] have proved to be a versatile technology both for the detection and identification of individual compounds[24−27] and for the discrimination among highly similar complex mixtures[28−30] in both gaseous or aqueous phases. The colorimetric sensor array differs fundamentally from traditional electronic nose techniques in that the sensor signals depend not on physical sorption of analyte molecules (inducing changes in the mass or conductivity) but instead on strong chemical interactions to change the color (i.e., UV−vis absorption) of a chemically diverse range of responsive dyes. These disposable colorimetric sensor arrays overcome the limitations that traditional electronic noses commonly suffer from, including sensor drift, poor chemical selectivity and sensitivity, and interference from changes in relative humidity.[21,31]

For this work, we designed new nanostructured materials as colorimetric sensors for the specific detection of volatile amines. Our sensor arrays on hydrophobic membranes were printed with chemically responsive inks made from nanoporous organically modified silica (ormosil) microspheres. The colors of these silica-dye composite nanoporous materials are highly responsive to amine analytes but insensitive to changes in ambient humidity. Ultrasonic spray pyrolysis (USP) provided a simple, scalable, and continuous method for the synthesis of these porous materials. The USP process consists of (1) nebulization of precursor solutions, (2) evaporation of droplets in the heated zone, (3) hydrolysis and condensation of siloxyl precursors, and (4) escape of product volatiles.[32] The highly porous, well-defined spherical (∼1 μm diameter) silica-dye composites facilitate gas exposure and improve sensor array response compared to the sensor made from the usual amorphous sol−gel suspensions.

We demonstrate herein a rapid, portable, and sensitive method for quantification of TMAO in simulated urine. The TMAO was chemically reduced to TMA, which is volatile, and the head gas was subsequently analyzed using a colorimetric sensor array in a palm-sized analyzer.[23]

2. EXPERIMENTAL SECTION

2.1. Reagents and Materials. All chemical reagents, including tetraethoxysilane (TEOS), ethyltriethoxysilane (ETES), octyl-triethoxysilane (OTES), and (2-phenylethyl)triethoxysilane (PTES), and 13 organic dyes (Table S1) were used as received unless otherwise specified. Simulated urine was prepared by incorporating inorganic and organic components according to the literature (cf. Table S2).[33−40]

2.2. Simulated Urine Pretreatment and Analysis. A protocol for the pretreatment of a simulated urine sample to remove volatile amines and the analysis of TMAO is shown in Scheme 2: (i) a small volume (10 μL) of simulated urine was dropped on a 5 × 1 cm filter paper strip (Whatman, Cat. no. 1450070), which was clamped and placed on a bench to dry for 2 min at ambient condition; (ii) the paper strip was transferred to a 7 mL scintillation vial, then 150 μL of deionized water was added into the vial to completely immerse the paper strip; (iii) 0.1 mg of Raney Ni/$NaBH_4$ mixture (1:4 w/w) was added to the solution, and the vial was capped immediately to collect the product for 2 min; and (iv) a handheld reader with an array was inserted halfway into the vial and sample the headspace gas through a Teflon feed tube for 2 min.

2.3. Preparation of Silica-Dye Microspheres. The sol−gel synthesis of porous silica-dye microspheres using a laboratory scalable ultrasonic setup is shown in Figure S1. In a typical synthesis, a precursor mixture of TEOS (2.08 g, 0.01 mol), with one of the organotriethoxysilanes (i.e., 0.02 mol of ETES, OTES, or PTES at 3.85, 5.53, or 5.37 g, respectively), ethanol (13 mL), nanopure water (26 mL), and aqueous HCl (1 mL, 0.1 M) were combined with 50 mg of each dye; the resulting solution is 0.25 M in TEOS, 0.5 M in organosilane, 2.5 mM in HCl, and ∼2 mM in dye. The precursor solution was introduced into an atomization cell and nebulized by a household ultrasonic humidifier (1.7 MHz, ∼10 W/cm^2). The resulting aerosol was carried by an Ar gas through a tube furnace at a temperature of 150, 300, or 450 °C; the Ar flow was set at 1.0 SLPM (standard liters per minute). The product was collected in a series of several bubblers containing 1:2 v/v mixture of ethanol and nanopure water and then centrifuged and washed with the same solvent mixtures three times to remove unencapsulated dyes. The final product, colored powders of silica-dye microspheres, was dispersed as chemically responsive inks in 9:1 mixtures of 2-methoxyethanol and polyethylene glycol (average $M_w \approx 3350$) prior to printing.

2.4. Material Characterization. For characterization of silica-dye microspheres, SEM was carried out using a Hitachi S-4700 operated at 10 kV; energy-dispersive X-ray spectroscopy (EDX) was coupled with a 7000F-SEM instrument using a Thermo Electron EDX microanalysis system. TEM was conducted using a JEOL 2100 Cryo instrument with an acceleration voltage of 200 kV. The Brunauer−Emmett−Teller (BET) specific surface areas were measured by a Quantachrome NOVA 2200e system. Powder XRD patterns were obtained on a Siemens−Bruker D-5000 XRD instrument operated at 40 kV and 30 mA (Cu Kα radiation).

2.5. Sensor Array Preparation. The linearized, 13-element colorimetric sensor arrays were prepared on polypropylene membranes with a robotic pin-printer, as described in detail elsewhere,[25] delivering 13 different inks containing nanoporous silica-dye microspheres. After printing, the arrays were put under vacuum for 1 h at room temperature and stored in N_2-filled Mylar bags before any measurements. The chemical dyes used in each spot are listed in Table S1.

2.6. Raw Data Process. Analyte responses were collected on a recently developed handheld reader[23] (Scheme 2) and calculated from the differences in red, green, and blue (ΔRGB) values of each sensor element by comparing after- to before-exposure images. For visualization purposes only, all color difference RGB values were expanded from 3 bits (i.e., 3−10) to 8 bits (i.e., 0−255). The signal-to-noise ratio (S/N) was calculated for each RGB channel and incorporated in the final database for statistical analysis, in which the signals were defined as the difference between each analyte trial measurement and the averaged nonexposed control of each data channel, and noise was defined as the standard deviation among quintuplicate trials of controls for each RGB channel.

2.7. Database Analysis. Two unsupervised statistical methods, principal component analysis (PCA), and hierarchical cluster analysis (HCA) were performed for database clustering using MVSP software (Kovach Computing Services, Pentraeth, Isle of Anglesey, UK); in all cases, minimum variance (i.e., "Ward's Method") was used for HCA clustering.

3. RESULTS AND DISCUSSION

Our aim in this project was to develop an inexpensive quantification of urinary TMAO that would be potentially useful as a point-of-care method for rapid, on-site, and early diagnosis of relevant diseases. We recognized that a multistep, but simple, process might be developed for the analysis of TMAO in complex biological samples with multiple amine components. The general steps of this process involve (1) removal of volatile amines (e.g., ammonia, dimethylamine, and TMA) from the simulated urine, (2) pretreatment of the solution TMAO using a reductant and catalyst, and (3) a sampling protocol for subsequently produced TMA. Specifically, an enzyme-free reagent (Raney Ni/$NaBH_4$) has been found to be an effective system for the highly selective

DOI: 10.1021/acsami.8b00995
ACS Appl. Mater. Interfaces 2018, 10, 15820−15828

deoxygenation of *N*-oxides in the aqueous phase, which permits the conversion of TMAO to TMA with a high yield (>95%) even at room temperature (Scheme 1) and in the presence of carbonyls (including urea, uric acid, creatine, or creatinine).[41]

Scheme 1. Reduction of TMAO Using Raney Ni/$NaBH_4$ Reagent

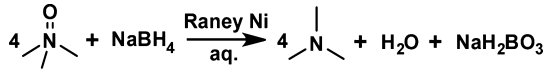

3.1. TMAO Analysis of Urine. Urine is a complicated biological sample that contains numerous inorganic or organic components. Volatile amines found in urine, including ammonia, methylamine, dimethylamine, ethylamine, and so on, are an important class of interferents in the analysis of TMAO. To eliminate such interferents, a simple protocol for analyzing a very small volume of simulated urine sample (10 μL) was developed (Scheme 2), which quickly dries out a urine-saturated filter paper strip to remove volatile amines, followed by redissolution of the remaining nonvolatile TMAO and other inorganic or organic nonvolatiles to regenerate an amine-free TMAO solution. On the basis of the overall sensor-array response, essentially all volatile amines were removed within 2 min (Scheme 2 and Figure S2). A reductant ($NaBH_4$ catalyzed by Raney Ni) was subsequently added to reduce TMAO to TMA for the analysis of the resulting release of the volatile amine.

Scheme 2. Procedures for the Removal of Volatile Amines, Reduction of TMAO, and Analysis of Newly Generated Amines in a Simulated Urine Sample[a]

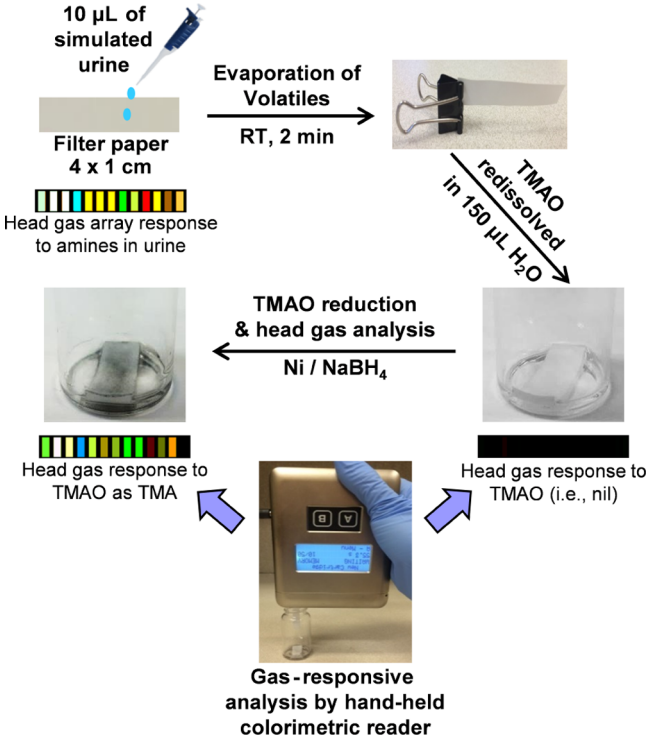

[a]The colored pattern under each sample vial (1 cm diameter) reflects the overall level of volatile amines as detected by the colorimetric sensor array and analyzed by the handheld device from the headspace gases of the vial.

The reaction rate is highly dependent on the amount of reductant used, but even at room temperature, TMAO can be completely reduced to TMA within 2 min, with the addition of 8 molar equivalents of $NaBH_4$ (Figure 1). The reductant is specific to *N*-oxide species[41] and shows no significant reaction during this procedure with the various carbonyl compounds that are abundant in urine (such as creatinine, a major metabolic waste produced in kidney, Figure S3).

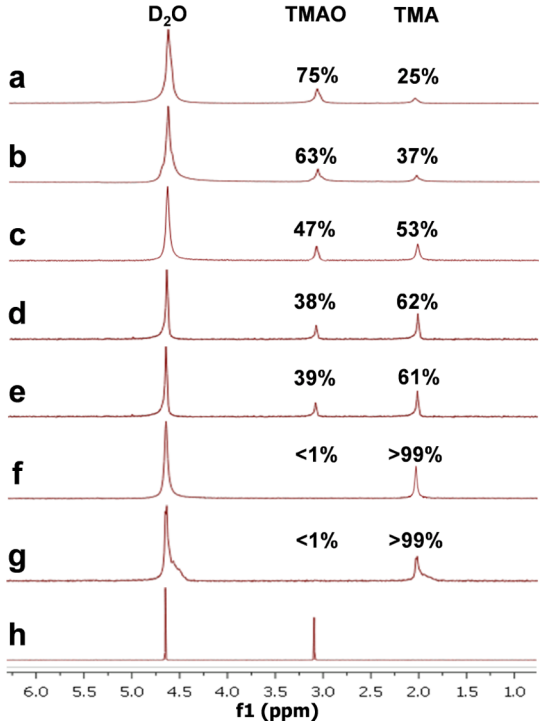

Figure 1. Reduction of TMAO to TMA at room temperature using Raney Ni/$NaBH_4$. NMR spectra of the reduction reaction after (a) 2; (b) 5; (c) 10; and (d) 15 min of a 1:2 molar ratio between TMAO and $NaBH_4$; after (e) 2 min and (f) 5 min of a 1:4 molar ratio between TMAO and $NaBH_4$; (g) 2 min of a 1:8 molar ratio between TMAO and $NaBH_4$; and (h) standard TMAO control without reduction. The reduction reaction is complete within 2 min when the molar ratio between TMAO and $NaBH_4$ is 1:8. In all cases, the starting concentration of TMAO was 200 μM, and the amount of Raney Ni was 0.1 mg/mL. Line broadening is due to presence of particulate Raney Ni catalyst.

3.2. Synthesis and Characterization of the Silica-Dye Microspheres. Factors that affect the performance of colorimetric sensor arrays in response to amines (i.e., response time, sensitivity, reproducibility, selectivity, or susceptibility to interferents) can be heavily influenced by the choice of substrates or sol–gel matrices of the colorants.[42,43] Over the past decade, we have been extensively using organically modified silicates prepared by a sol–gel method as host matrices for different sensor elements.[24,44] Compared to other porous materials, porous organosilica materials[45−49] provide an impressive set of physical and chemical properties including superior chemical resistance to acids or bases, higher heat durability, proper permeability, tunable hydrophobicity or porosity, ease of modification, and ideal optical transparency or reflectivity. These properties provide better control of the sensor media to ensure stable immobilization and solvation of colorants, ample accessibility of colorant centers to analytes,

DOI: 10.1021/acsami.8b00995
ACS Appl. Mater. Interfaces 2018, 10, 15820−15828

and prevention from leaching or blooming of the dye molecules. Taking advantage of these properties, porous silica matrices can also serve as potential in situ preconcentrators for analyte molecules, thus enhancing the overall sensitivity and kinetic response toward any gaseous or aqueous analytes.

The preparation of porous organosilica with well-defined nanostructure through a facile, tunable, and scalable approach is also of great importance for the exploration of new sensing materials. USP[32,50−52] is well-suited for the scalable production of organosilica micro- or nanoparticles. In a typical USP process, ultrasound is used to nebulize the precursor solution droplets carried in an inert carrier gas. The aerosol droplets are carried through a furnace, where evaporation of solvent and chemical reactions of the precursors occurs, so as to generate microscale or nanoscale solid products with generally spherical morphologies. Using low-volatility precursors, the reactions responsible for the formation of products are confined within each individual droplet. In this manner, the droplets formed during USP act as individual chemical microreactors that impose morphology control on the products.

To investigate into the effects of organic substituents and reaction conditions on the morphology of the ormosil microspheres products, USP syntheses were performed at different temperatures using siloxanes with ethyl, octyl, or 2-phenylethyl organic substituents with dyes incorporated by entrapment into the resulting sol−gel. It was previously reported that microspheres made of only TEOS are nonporous and impermeable, whereas products from ETES alone give high permeability with significant leaching of dye when the microspheres are resuspended in solvents.[44] This suggested the use of a mixture of TEOS and ETES to prevent dye leaching. To study the optimal combination of reactants, the reaction was conducted over a wide range of ETES/TEOS ratios at a relatively low temperature (150 °C); a typical pH indicator, bromocresol green (BCG), was incorporated in the aerosol−gel synthesis (the concentration of the dye, ∼2 mM, is sufficiently low that it does not affect the sol−gel formation). A molar ratio of 1:2 of ETES/TEOS produced the most responsive microspheres: printed spots show no color change in response to 1 ppm TMA vapor when no ETES was used as a reactant; as the proportion of ETES increases, the color change from yellow to green becomes increasingly apparent; and the highest response (defined by the Euclidean distance of ΔRGB vectors) is obtained on the spot with a 1:2 molar ratio; such a color change tends to be weaker as the amount of ETES is increased further (Figure S4a). The optimal ratio of two precursors is a compromise between the accessibility of analytes to dyes and the capability of dye encapsulation: as the permeability of the sensor matrices increases, quicker response time or higher equilibrated response is expected, but colorants become prone to leaching during workup that diminishes the overall sensitivity.

The impact of reaction temperature on the physical properties and responsiveness of the silica-dye microspheres was also examined. Furnace temperatures of 150, 300, or 450 °C were used to prepare silica-dye microspheres with a 1:2 molar ratio of TEOS and ETES doped with BCG. TEM and SEM micrographs show that hollow, porous microspheres (647 ± 60 nm in diameter) with smooth surfaces were obtained at 150 °C (Figure 2a−c); as the temperature goes up to 300 and 450 °C, particles formed are more solid and less smooth (Figure 2d−i). The size of microspheres shrink modestly to 582 ± 55 nm at 300 and 519 ± 68 nm at 450 °C. BET-specific

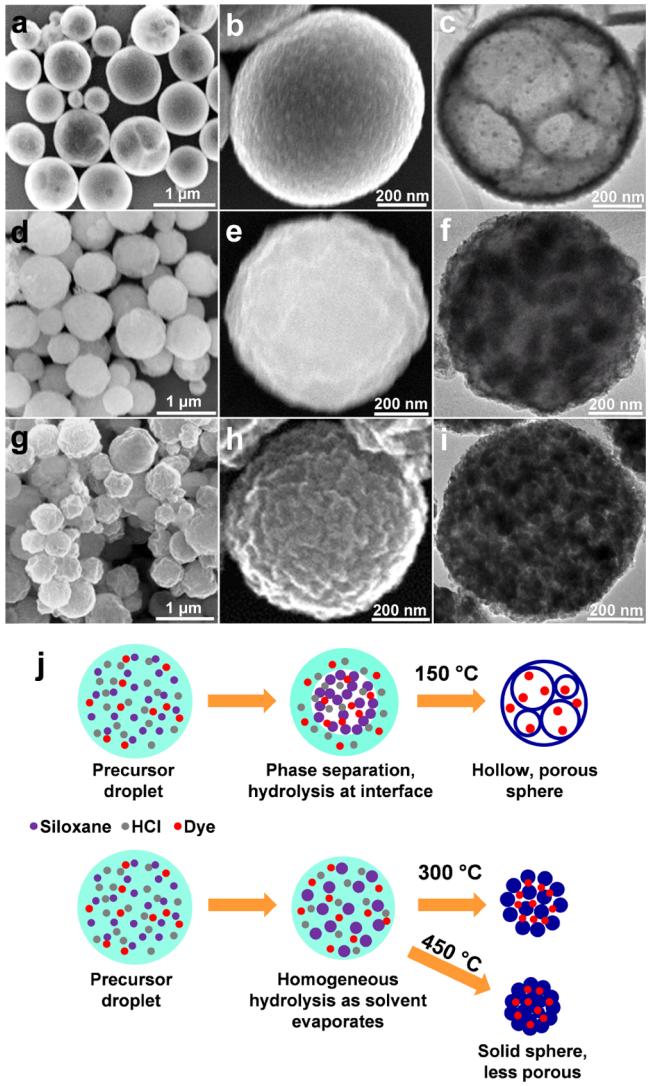

Figure 2. SEM (a,b,d,e,g,h) and TEM (c,f,i) micrographs of nanoporous silica-dye microspheres synthesized from TEOS and ETES at three different temperatures: (a−c) 150 °C; (d−f) 300 °C; and (g−i) 450 °C; the diameters of as-synthesized microspheres are 650, 580, and 520 nm, respectively; and (j) proposed mechanisms for the formation of silica-dye microspheres at different temperatures. The porosity of microspheres diminishes as the temperature increases (surface areas of 310, 156, and 91 m^2/g at 150, 300, and 450 °C, respectively).

surface areas of the microspheres synthesized at 150, 300, and 450 °C are 310, 156, and 91 m^2/g, respectively, which shows reduced porosity for microspheres formed at higher temperatures. The colorimetric sensitivity of these microspheres to TMA improves with increased porosity (Figure S4b).

On the basis of particle morphologies, we propose a mechanism for the formation of microspheres (Figure 2j): at lower temperatures, the precursor solution undergoes a phase-separation process between H_2O and insoluble siloxanes, and hydrolysis is therefore occurring at the aqueous−organic interfaces, which leads to hollow spheres as products; under higher temperature conditions, a more homogeneous hydrolysis and subsequent pyrolysis lead to partial collapse of the surface pores of microspheres, diminishing both their size and their porosity, which diminishes the access of analytes from the encapsulated dye molecules in the silica matrices. Elemental

DOI: 10.1021/acsami.8b00995
ACS Appl. Mater. Interfaces 2018, 10, 15820−15828

mapping using EDX (i.e., X-ray emissions from K_α lines of S and Br from the dyes compared to that of Si K_α) demonstrates an even distribution of dye molecules in the silica-host matrices synthesized at 150 °C (Figure 3).

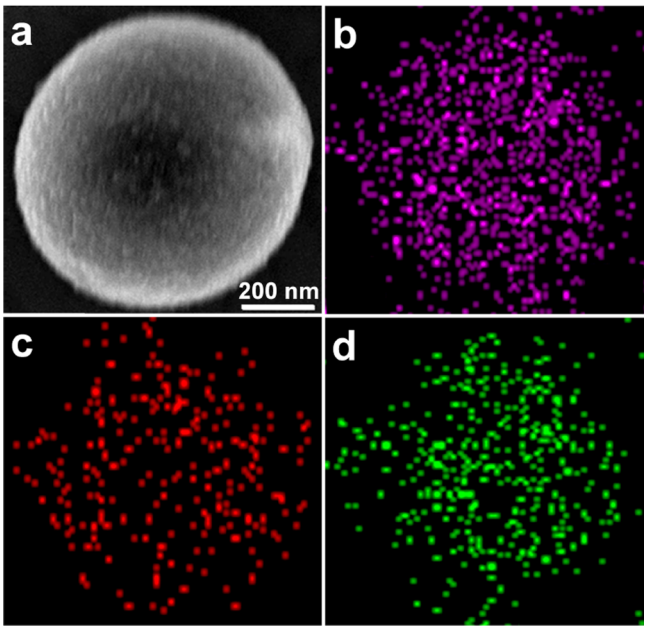

Figure 3. (a) SEM micrograph of a single microsphere prepared at 150 °C from the mixture of TEOS, ETES, and BCG, and EDX elemental mapping of (b) Si, (c) S, and (d) Br, calculated from Kα emission lines.

As a control experiment to study the influence of the size of the hydrocarbon substituent of the siloxane on the particle porosity, the other two organically modified triethoxysilane precursors with bulkier substituents, OTES and PTES, were used with TEOS at 150 °C; decreased reactivity was observed as the substituent size grows (Figure S4c), which matches well with the trend in BET surface areas of the microspheres: ETES (310 m^2/g), OTES (217 m^2/g), and PTES (172 m^2/g). The N_2 adsorption–desorption isotherms show type II hysteresis loops of all three materials (Figure 4a). The absence of characteristic peaks in powder XRD patterns confirms amorphous polymeric structures for all three microspheres (Figure S5).

The high-resolution TEM images (Figure S6) show that a substantial number of nanopores (~1–2 nm in diameter) are present in the SiO_2-BCG microspheres obtained from the TEOS/ETES precursor mixture at 150 °C but not from TEOS/OTES or TEOS/PTES precursors. The nanostructure contributes to their improved surface area and consequently, enhanced gas-sensing property. This observation is consistent with the pore size distribution of three microspheres, calculated by the Barrett–Joyner–Halenda (BJH) model (Figure 4b).[53] The predominant distribution of the material from TEOS and ETES centered at 1.3 nm indicates its high surface area and superior capability of analyte exposure to the encapsulated dye.

3.3. Colorimetric Array Responses. Thirteen different amine-sensitive dyes were selected from our prior work on colorimetric sensor arrays,[26] and each of them was incorporated into the silica microspheres made of TEOS and ETES under the optimized synthetic conditions. The suspensions of each of the as-synthesized silica-dye microspheres were dispersed in ethanol and pin-printed on a polypropylene membrane as a

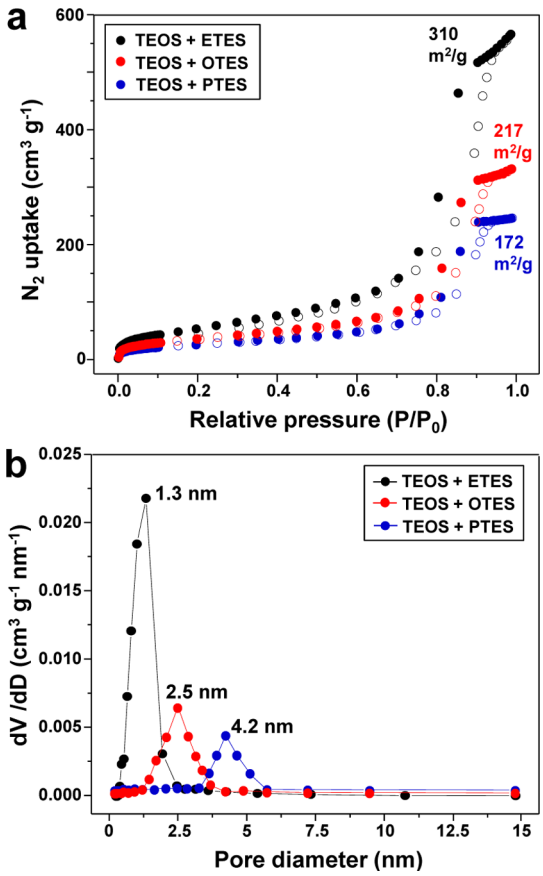

Figure 4. (a) N_2 adsorption–desorption isotherms of three microspheres made from siloxanes modified with different substituents. (b) Pore-size distributions of three microspheres made from different siloxanes according to the Barrett–Joyner–Halenda (BJH) model. All data were measured with N_2 at 77 K.

linear array of colorimetric sensors. The headspace vapors present in a vial containing TMA produced from the reduction of TMAO (as per Scheme 2) were sampled over the array, whose responses were imaged and analyzed by an inexpensive, self-contained handheld scanner.[23]

Figure 5a shows colorimetric sensor responses to a series of concentrations of TMAO spiked in simulated urine samples after 2 min exposure to the headspace volatiles. Significant color changes were observed by the naked eye even down to micromolar levels of TMAO. The biggest responses are from solvatochromic dyes (spots 1 and 2), pH indicators (spots 3–11), and metal-containing dyes (spots 12 and 13), which reflects the changes in local polarity, Brønsted basicity, and Lewis basicity created by the presence of TMA vapor. Color difference maps as a function of TMAO concentration in the simulated urine samples are readily distinguishable from one another even by eye before any statistical analysis.

To demonstrate the improvement in sensor response because of the sensor's nanostructure, a control experiment was conducted to prepare simple silica-dye composite colloids (i.e., not porous microspheres) via ordinary magnetic stirring using the same reactants: 1:2 molar mixture of TEOS and ETES plus each of the 13 dyes stirred at room temperature. The as-synthesized silica-dye composites show neither nanopores (Figure S7) nor comparably high specific surface areas. Thirteeen dye-doped silica suspensions were similarly deposited on the polymer membrane as the sensor array and tested

DOI: 10.1021/acsami.8b00995
ACS Appl. Mater. Interfaces 2018, 10, 15820–15828

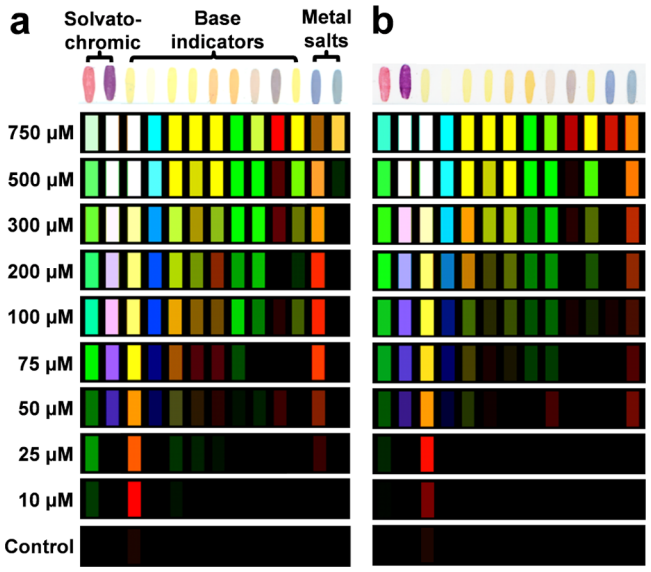

Figure 5. Color difference profiles of the sensor array made from (a) 13 silica-dye nanoporous microspheres and (b) stirred silica-dye suspensions with the same set of dyes after 2 min exposure of amine vapors from the reduction of TMAO at different urinary concentrations. A significant color change was still observed at 10 μM. For display purposes only, color difference RGB values were expanded from 3 to 8 bits.

against amine vapors from the reduction of TMAO solutions. As shown in Figure 6, stirred silica suspensions were somewhat

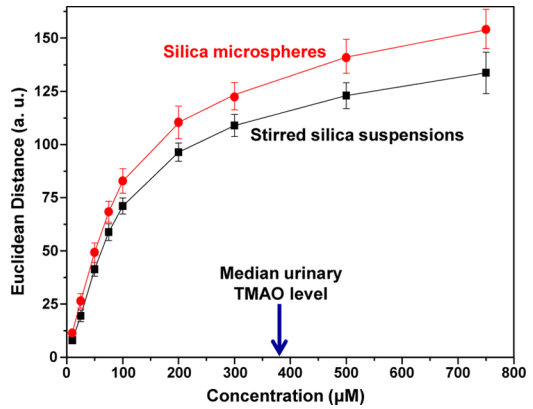

Figure 6. Response curves of sensor arrays made of silica-dye microspheres or stirred suspensions to products from reduced TMAO over a wide range of concentrations; the median urinary level of TMAO for healthy subjects is ~380 μM. The response at each concentration from nanoporous silica microspheres are 15–20% higher than the simple silica colloids.

less responsive (by ~15–20%) than nanoporous microspheres at each concentration of spiked TMAO after 2 min exposure of generated volatile amine. The high surface area of silica microspheres with well-defined nanostructure and suitable permeability is beneficial in providing the increased surface area and therefore improved contact with analytes, resulting in enhanced sensor response to gaseous amines.

The limit of detection (LOD) for urinary TMAO was calculated by linearly fitting the data points between 10 and 100 μM (which gives a good linearity, $R^2 = 0.993$) and extrapolating the curve to the concentration, where the sensor response is 3 times that of the noise level (i.e., S/N = 3), as shown in Figure S8. The calculation was based on the most responsive ΔRGB value (i.e., the red channel of spot 3, which even responds to 10 μM TMAO), instead of the overall Euclidean distance of all sensors, to achieve a better precision of the estimated LOD. An LOD of ~4 μM for TMAO in the simulated urine matrix was obtained, which is well-below the median urinary level of TMAO from healthy subjects (~380 μM).[54]

3.4. Multivariate Analysis. We made use of two standard chemometric methods, HCA and PCA,[55,56] to group colorimetric data of all TMAO concentrations. As a semi-quantitative evaluation of the array responses, the advantages of HCA are that it is intrinsically model-free (i.e., unsupervised) and that it deals well with high-dimensional data.[21] The clustering of vectors is based on their positions in the 39-dimension Euclidean space (i.e., changes in RGB differences for each of the 13 sensor elements). The resultant dendrogram reflects the relative distances among analyte responses. Figure 7

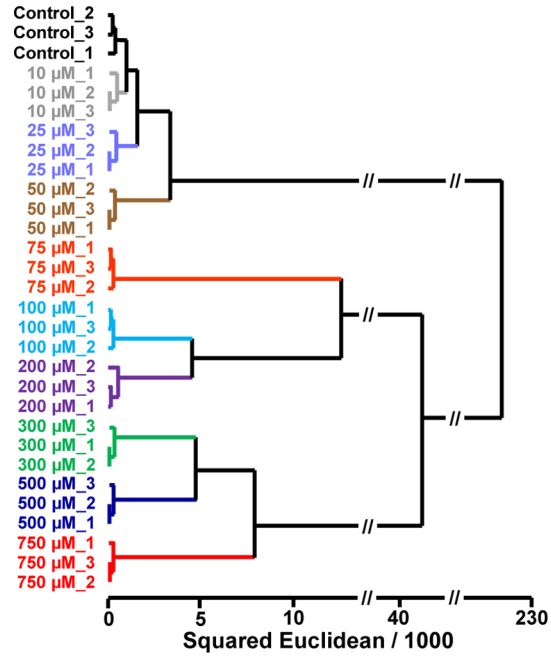

Figure 7. Dendrogram of HCA showing the accurate clustering of all concentrations of urinary TMAO plus a control (no TMAO spiked).

shows the HCA dendrogram for 2 min exposure to headspace gases from the reduction of TMAO solutions in simulated urine at nine different concentrations. Tight clustering at each concentration plus a non-TMAO control was observed with no errors out of triplicate trials of each sample (30 cases in total).

PCA was performed to provide a measurement of the dimensionality of the data. As another model-free statistical method, PCA aims to create linear combination of the raw data so as to maximize the total variance in as few dimensions as possible. Given the very limited range of chemical diversity present among different concentrations of the same analyte (i.e., TMA vapors from TMAO), relatively low dimensionality was expected and indeed observed: three dimensions are responsible for >90% of the total variance and five dimensions are required to capture >95% of the total variance (Figure S9a). Similar to clustering results of HCA dendrogram, the PCA score plot shows excellent separation among concentrations even using just the first two principal components (Figure

DOI: 10.1021/acsami.8b00995
ACS Appl. Mater. Interfaces 2018, 10, 15820–15828

S9b). It is noteworthy that the PCA is heavily dominated by a single principal component (i.e., axis 1, 71.7% of total variance), and that dimension essentially represents the concentration of the TMA vapor. As a result, the analyte clusters distribute primarily along that dimension as a function of the TMAO concentration.

3.5. Sensor Array Optimization. Simplicity of a sensor array is sometimes important to their practical use in the field. To simplify the procedures needed for sensor fabrication and data analysis, the number of sensors in the array can be further reduced without diminishing the overall selectivity of the array, especially in the case of TMAO urine analysis, where chemical specificity is not likely to be a serious issue. The only source of volatile amines detected is from the reduction of TMAO, and no significant concentrations of interferents are generally expected. Therefore, it is feasible to monitor the concentration of TMA (and hence TMAO before reduction) by the use of a limited number of sensor elements that are highly sensitive to amines. The Euclidean distance of each of the eight most responsive spots from the array was plotted as a function of TMAO concentrations, which shows that spot 1 (containing α-naphthyl red) and 3 (containing tetraiodophenolsulfonephthalein) are the top two most-responsive sensors in response to TMA (Figure S10). For some applications involving TMAO quantification, one might wish to simplify the sensor array to one, two, or perhaps three of the most responsive sensor spots.

4. CONCLUSIONS

In conclusion, an effective method for rapid quantification of TMAO in urine (<6 min) was demonstrated by converting TMAO (a nonvolatile, chemically inert analyte) into volatile TMA using a simple catalytic reduction. A 13-element colorimetric sensor array consisting of organically modified silica-dye microspheres prepared by USP was fabricated and tested against a series of clinically significant concentrations of TMAO in simulated urine samples. Statistical analyses, including hierarchical cluster analysis and PCA, give classification of all tested concentrations without error. The calibration curve gives a linear response range of 10−100 μM and a detection limit of ∼4 μM, which is well-below the median urinary concentrations of TMAO among healthy subjects. Our device may prove effective in the early diagnosis of TMAO-relevant diseases associated with circulatory or digestive systems and may find promising applications as a point-of-care tool for rapid, inexpensive detection of TMAO in biological samples such as urine or serum.

■ ASSOCIATED CONTENT

Supporting Information

The Supporting Information is available free of charge on the ACS Publications website at DOI: 10.1021/acsami.8b00995.

Dye formulations, experimental details, sensor response graphs, statistical analysis, and all raw data (PDF)

■ AUTHOR INFORMATION

Corresponding Author

*E-mail: ksuslick@illinois.edu.

ORCID

Zheng Li: 0000-0001-9066-5791

Kenneth S. Suslick: 0000-0001-5422-0701

Notes

The authors declare no competing financial interest.

■ ACKNOWLEDGMENTS

Z.L. acknowledges the postdoctoral financial support from the Procter & Gamble Foundation (085310) and helpful discussions with Drs. Xiaole Mao and Sherman Faiz from Procter & Gamble. This work was carried out in part in the Frederick Seitz Materials Research Laboratory Central Facilities at the University of Illinois.

■ REFERENCES

(1) Velasquez, M.; Ramezani, A.; Manal, A.; Raj, D. Trimethylamine N-Oxide: The Good, the Bad and the Unknown. *Toxins* **2016**, *8*, 326.

(2) Cho, C. E.; Caudill, M. A. Trimethylamine-*N*-Oxide: Friend, Foe, or Simply Caught in the Cross-Fire? *Trends Endocrinol. Metab.* **2017**, *28*, 121−130.

(3) Lever, M.; George, P. M.; Slow, S.; Bellamy, D.; Young, J. M.; Ho, M.; McEntyre, C. J.; Elmslie, J. L.; Atkinson, W.; Molyneux, S. L.; Troughton, R. W.; Frampton, C. M.; Richards, A. M.; Chambers, S. T. Betaine and Trimethylamine-N-Oxide as Predictors of Cardiovascular Outcomes Show Different Patterns in Diabetes Mellitus: An Observational Study. *PLoS One* **2014**, *9*, e114969.

(4) Xu, K.-Y.; Xia, G.-H.; Lu, J.-Q.; Chen, M.-X.; Zhen, X.; Wang, S.; You, C.; Nie, J.; Zhou, H.-W.; Yin, J. Impaired Renal Function and Dysbiosis of Gut Microbiota Contribute to Increased Trimethylamine-N-Oxide in Chronic Kidney Disease Patients. *Sci. Rep.* **2017**, *7*, 1445.

(5) Liu, X.; Liu, H.; Yuan, C.; Zhang, Y.; Wang, W.; Hu, S.; Liu, L.; Wang, Y. Preoperative Serum Tmao Level Is a New Prognostic Marker for Colorectal Cancer. *Biomarkers Med.* **2017**, *11*, 443−447.

(6) Xu, R.; Wang, Q.; Li, L. A Genome-Wide Systems Analysis Reveals Strong Link between Colorectal Cancer and Trimethylamine N-Oxide (Tmao), a Gut Microbial Metabolite of Dietary Meat and Fat. *BMC Genomics* **2015**, *16*, S4.

(7) Bennett, B. J.; de Aguiar Vallim, T. Q.; Wang, Z.; Shih, D. M.; Meng, Y.; Gregory, J.; Allayee, H.; Lee, R.; Graham, M.; Crooke, R.; Edwards, P. A.; Hazen, S. L.; Lusis, A. J. Trimethylamine-N-Oxide, a Metabolite Associated with Atherosclerosis, Exhibits Complex Genetic and Dietary Regulation. *Cell Metab.* **2013**, *17*, 49−60.

(8) Ierardi, E.; Sorrentino, C.; Principi, M.; Giorgio, F.; Losurdo, G.; Di Leo, A. Intestinal Microbial Metabolism of Phosphatidylcholine: A Novel Insight in the Cardiovascular Risk Scenario. *Hepatobiliary Surg. Nutr.* **2015**, *4*, 289−292.

(9) Gruppen, E. G.; Garcia, E.; Connelly, M. A.; Jeyarajah, E. J.; Otvos, J. D.; Bakker, S. J. L.; Dullaart, R. P. F. Tmao Is Associated with Mortality: Impact of Modestly Impaired Renal Function. *Sci. Rep.* **2017**, *7*, 13781.

(10) Senthong, V.; Wang, Z.; Fan, Y.; Wu, Y.; Hazen, S. L.; Tang, W. H. W. Trimethylamine N-Oxide and Mortality Risk in Patients with Peripheral Artery Disease. *J. Am. Heart Assoc.* **2016**, *5*, e004237.

(11) Randrianarisoa, E.; Lehn-Stefan, A.; Wang, X.; Hoene, M.; Peter, A.; Heinzmann, S. S.; Zhao, X.; Königsrainer, I.; Königsrainer, A.; Balletshofer, B.; Machann, J.; Schick, F.; Fritsche, A.; Häring, H.-U.; Xu, G.; Lehmann, R.; Stefan, N. Relationship of Serum Trimethylamine N-Oxide (Tmao) Levels with Early Atherosclerosis in Humans. *Sci. Rep.* **2016**, *6*, 26745.

(12) Wang, Z.; Levison, B. S.; Hazen, J. E.; Donahue, L.; Li, X.-M.; Hazen, S. L. Measurement of Trimethylamine-N-Oxide by Stable Isotope Dilution Liquid Chromatography Tandem Mass Spectrometry. *Anal. Biochem.* **2014**, *455*, 35−40.

(13) Awwad, H. M.; Geisel, J.; Obeid, R. Determination of Trimethylamine, Trimethylamine N-Oxide, and Taurine in Human Plasma and Urine by Uhplc−Ms/Ms Technique. *J. Chromatogr. B: Anal. Technol. Biomed. Life Sci.* **2016**, *1038*, 12−18.

(14) Heaney, L. M.; Jones, D. J. L.; Mbasu, R. J.; Ng, L. L.; Suzuki, T. High Mass Accuracy Assay for Trimethylamine N-Oxide Using Stable-Isotope Dilution with Liquid Chromatography Coupled to Orthogonal

DOI: 10.1021/acsami.8b00995
ACS Appl. Mater. Interfaces 2018, 10, 15820−15828

Acceleration Time of Flight Mass Spectrometry with Multiple Reaction Monitoring. *Anal. Bioanal. Chem.* **2016**, *408*, 797−804.
(15) Zhao, X.; Zeisel, S. H.; Zhang, S. Rapid Lc-Mrm-Ms Assay for Simultaneous Quantification of Choline, Betaine, Trimethylamine, Trimethylamine N-Oxide, and Creatinine in Human Plasma and Urine. *Electrophoresis* **2015**, *36*, 2207−2214.
(16) Taesuwan, S.; Cho, C. E.; Malysheva, O. V.; Bender, E.; King, J. H.; Yan, J.; Thalacker-Mercer, A. E.; Caudill, M. A. The Metabolic Fate of Isotopically Labeled Trimethylamine-N-Oxide (Tmao) in Humans. *J. Nutr. Biochem.* **2017**, *45*, 77−82.
(17) Garcia, E.; Wolak-Dinsmore, J.; Wang, Z.; Li, X. S.; Bennett, D. W.; Connelly, M. A.; Otvos, J. D.; Hazen, S. L.; Jeyarajah, E. J. Nmr Quantification of Trimethylamine-N-Oxide in Human Serum and Plasma in the Clinical Laboratory Setting. *Clin. Biochem.* **2017**, *50*, 947−955.
(18) Podadera, P.; Arêas, J. A. G.; Lanfer-Marquez, U. M. Diagnosis of Suspected Trimethylaminuria by Nmr Spectroscopy. *Clin. Chim. Acta* **2005**, *351*, 149−154.
(19) Hatton, A. D.; Gibb, S. W. A Technique for the Determination of Trimethylamine-N-Oxide in Natural Waters and Biological Media. *Anal. Chem.* **1999**, *71*, 4886−4891.
(20) Sadok, S.; Uglow, R. F.; Haswell, S. J. Determination of Trimethylamine Oxide in Seawater and Small Volumes of Seafood Tissue Extract Using Flow Injection Analysis. *Anal. Chim. Acta* **1996**, *334*, 279−285.
(21) Askim, J. R.; Mahmoudi, M.; Suslick, K. S. Optical Sensor Arrays for Chemical Sensing: The Optoelectronic Nose. *Chem. Soc. Rev.* **2013**, *42*, 8649−8682.
(22) Rakow, N. A.; Suslick, K. S. A Colorimetric Sensor Array for Odour Visualization. *Nature* **2000**, *406*, 710−713.
(23) Askim, J. R.; Suslick, K. S. Hand-Held Reader for Colorimetric Sensor Arrays. *Anal. Chem.* **2015**, *87*, 7810−7816.
(24) Lim, S. H.; Feng, L.; Kemling, J. W.; Musto, C. J.; Suslick, K. S. An Optoelectronic Nose for the Detection of Toxic Gases. *Nat. Chem.* **2009**, *1*, 562−567.
(25) Li, Z.; Fang, M.; LaGasse, M. K.; Askim, J. R.; Suslick, K. S. Colorimetric Recognition of Aldehydes and Ketones. *Angew. Chem., Int. Ed.* **2017**, *56*, 9860−9863.
(26) Li, Z.; Li, H.; LaGasse, M. K.; Suslick, K. S. Rapid Quantification of Trimethylamine. *Anal. Chem.* **2016**, *88*, 5615−5620.
(27) Musto, C. J.; Lim, S. H.; Suslick, K. S. Colorimetric Detection and Identification of Natural and Artificial Sweeteners. *Anal. Chem.* **2009**, *81*, 6526−6533.
(28) Suslick, B. A.; Feng, L.; Suslick, K. S. Discrimination of Complex Mixtures by a Colorimetric Sensor Array: Coffee Aromas. *Anal. Chem.* **2010**, *82*, 2067−2073.
(29) Li, Z.; Bassett, W. P.; Askim, J. R.; Suslick, K. S. Differentiation among Peroxide Explosives with an Optoelectronic Nose. *Chem. Commun.* **2015**, *51*, 15312−15315.
(30) Li, Z.; Suslick, K. S. Portable Optoelectronic Nose for Monitoring Meat Freshness. *ACS Sens.* **2016**, *1*, 1330−1335.
(31) Röck, F.; Barsan, N.; Weimar, U. Electronic Nose: Current Status and Future Trends. *Chem. Rev.* **2008**, *108*, 705−725.
(32) Xu, H.; Zeiger, B. W.; Suslick, K. S. Sonochemical Synthesis of Nanomaterials. *Chem. Soc. Rev.* **2013**, *42*, 2555−2567.
(33) Wolrath, H.; Stahlbom, B.; Hallen, A.; Forsum, U. Trimethylamine and Trimethylamine Oxide Levels in Normal Women and Women with Bacterial Vaginosis Reflect a Local Metabolism in Vaginal Secretion as Compared to Urine. *APMIS* **2005**, *113*, 513−516.
(34) Lundh, T.; Åkesson, B. Gas Chromatographic Determination of Primary and Secondary Low-Molecular-Mass Aliphatic Amines in Urine Using Derivatization with Isobutyl Chloroformate. *J. Chromatogr. B: Biomed. Sci. Appl.* **1993**, *617*, 191−196.
(35) Tang, W. H. W.; Wang, Z.; Levison, B. S.; Koeth, R. A.; Britt, E. B.; Fu, X.; Wu, Y.; Hazen, S. L. Intestinal Microbial Metabolism of Phosphatidylcholine and Cardiovascular Risk. *N. Engl. J. Med.* **2013**, *368*, 1575−1584.
(36) Tsikas, D.; Thum, T.; Becker, T.; Pham, V. V.; Chobanyan, K.; Mitschke, A.; Beckmann, B.; Gutzki, F.-M.; Bauersachs, J.; Stichtenoth, D. O. Accurate Quantification of Dimethylamine (Dma) in Human Urine by Gas Chromatography−Mass Spectrometry as Pentafluorobenzamide Derivative: Evaluation of the Relationship between Dma and Its Precursor Asymmetric Dimethylarginine (Adma) in Health and Disease. *J. Chromatogr. B: Anal. Technol. Biomed. Life Sci.* **2007**, *851*, 229−239.
(37) Barr, D. B.; Wilder, L. C.; Caudill, S. P.; Gonzalez, A. J.; Needham, L. L.; Pirkle, J. L. Urinary Creatinine Concentrations in the U.S. Population: Implications for Urinary Biologic Monitoring Measurements. *Environ. Health Perspect.* **2005**, *113*, 192−200.
(38) Pandey, S.; Nanda, K. K. Au Nanocomposite Based Chemiresistive Ammonia Sensor for Health Monitoring. *ACS Sens.* **2016**, *1*, 55−62.
(39) Artificial Urine, http://www.pickeringtestsolutions.com/catalog/AU.php, accessed: Nov 22, 2017.
(40) Kim, W.; Tengra, F. K.; Young, Z.; Shong, J.; Marchand, N.; Chan, H. K.; Pangule, R. C.; Parra, M.; Dordick, J. S.; Plawsky, J. L.; Collins, C. H. Spaceflight Promotes Biofilm Formation by Pseudomonas Aeruginosa. *PLoS One* **2013**, *8*, e62437.
(41) Gowda, N. B.; Rao, G. K.; Ramakrishna, R. A. A Chemoselective Deoxygenation of N-Oxides by Sodium Borohydride−Raney Nickel in Water. *Tetrahedron Lett.* **2010**, *51*, 5690−5693.
(42) Tseng, S.-Y.; Li, S.-Y.; Yi, S.-Y.; Sun, A. Y.; Gao, D.-Y.; Wan, D. Food Quality Monitor: Paper-Based Plasmonic Sensors Prepared through Reversal Nanoimprinting for Rapid Detection of Biogenic Amine Odorants. *ACS Appl. Mater. Interfaces* **2017**, *9*, 17306−17316.
(43) Chen, Y.; Liu, L.; Xu, L.; Song, S.; Kuang, H.; Cui, G.; Xu, C. Gold Immunochromatographic Sensor for the Rapid Detection of Twenty-Six Sulfonamides in Foods. *Nano Res.* **2017**, *10*, 2833−2844.
(44) Bang, J. H.; Lim, S. H.; Park, E.; Suslick, K. S. Chemically Responsive Nanoporous Pigments: Colorimetric Sensor Arrays and the Identification of Aliphatic Amines. *Langmuir* **2008**, *24*, 13168−13172.
(45) *Optical Chemical Sensors*; Baldini, F., Chester, A. N., Homola, J., Martellucci, S., Eds.; Springer: Netherlands, Dordrecht, 2006.
(46) Carrington, N. A.; Xue, Z.-L. Inorganic Sensing Using Organofunctional Sol-Gel Materials. *Acc. Chem. Res.* **2007**, *40*, 343−350.
(47) Burleigh, M. C.; Markowitz, M. A.; Spector, M. S.; Gaber, B. P. Porous Organosilicas: An Acid-Catalyzed Approach. *Langmuir* **2001**, *17*, 7923−7928.
(48) Du, G.; Peng, J.; Zhang, Y.; Zhang, H.; Lü, J.; Fang, Y. One-Step Synthesis of Hydrophobic Multicompartment Organosilica Microspheres with Highly Interconnected Macro-Mesopores for the Stabilization of Liquid Marbles with Excellent Catalysis. *Langmuir* **2017**, *33*, 5223−5235.
(49) Chen, F.; Zhao, E.; Kim, T.; Wang, J.; Hableel, G.; Reardon, P. J. T.; Ananthakrishna, S. J.; Wang, T.; Arconada-Alvarez, S.; Knowles, J. C.; Jokerst, J. V. Organosilica Nanoparticles with an Intrinsic Secondary Amine: An Efficient and Reusable Adsorbent for Dyes. *ACS Appl. Mater. Interfaces* **2017**, *9*, 15566−15576.
(50) Skrabalak, S. E.; Suslick, K. S. Porous Mos2 Synthesized by Ultrasonic Spray Pyrolysis. *J. Am. Chem. Soc.* **2005**, *127*, 9990−9991.
(51) Bang, J. H.; Helmich, R. J.; Suslick, K. S. Nanostructured Zns:Ni2+ Photocatalysts Prepared by Ultrasonic Spray Pyrolysis. *Adv. Mater.* **2008**, *20*, 2599−2603.
(52) Ye, Z.; Yang, J.; Li, B.; Shi, L.; Ji, H.; Song, L.; Xu, H. Amorphous Molybdenum Sulfide/Carbon Nanotubes Hybrid Nanospheres Prepared by Ultrasonic Spray Pyrolysis for Electrocatalytic Hydrogen Evolution. *Small* **2017**, *13*, 1700111.
(53) Barrett, E. P.; Joyner, L. G.; Halenda, P. P. The Determination of Pore Volume and Area Distributions in Porous Substances. I. Computations from Nitrogen Isotherms. *J. Am. Chem. Soc.* **1951**, *73*, 373−380.
(54) Svensson, B. G.; Åkesson, B.; Nilsson, A.; Paulsson, K. Urinary Excretion of Methylamines in Men with Varying Intake of Fish from the Baltic Sea. *J. Toxicol. Environ. Health* **1994**, *41*, 411−420.
(55) Janata, J. *Principles of Chemical Sensors*, 2nd ed.; Springer: New York, 2009.

DOI: 10.1021/acsami.8b00995
ACS Appl. Mater. Interfaces 2018, 10, 15820−15828

(56) Hair, J. F.; Black, B.; Babin, B.; Anderson, R. E.; Tatham, R. L. *Multivariate Data Analysis*, 6th ed.; Prentice Hall: New York, 2005.

DOI: 10.1021/acsami.8b00995
ACS Appl. Mater. Interfaces 2018, 10, 15820−15828